

Optical quantum memory based on electro-optically silenced photon echo

Xia-Xia Li, Pai Zhou, Yu-Hui Chen,* and Xiangdong Zhang†

School of physics, Beijing Institute of Technology, Haidian District, Beijing 100081, People's Republic of China

(Dated: June 15, 2022)

Integrated quantum memories are a scalable solution to synchronize a large number of quantum computers, which are essential to build a quantum network to boost their capabilities on information processing. Rather than expecting to find a specific kind of atoms to meet all the requirements of a good quantum memory, as other protocols usually do, we propose that assigning the memory requirements on coherence property and control property to rare earth ions and lithium niobate crystal, respectively. In particular, optical quantum states are stored into erbium doped lithium niobate ($\text{Er}^{3+}:\text{LiNbO}_3$) micro-cavity by utilizing the electro-optic effect of LiNbO_3 . The $\text{Er}^{3+}:\text{LiNbO}_3$ cavity frequency can be shifted by an external electric field, which is used to control the photon-echo emission by changing the resonance condition between micro-cavity and collective atomic excitation. According to calculations, high efficiency and low noise storage can be achieved. Benefiting from the host lithium-niobate thin film, such a device can be controlled by on-chip electrodes and is easy to be integrated with modern photonic devices, paving way of integrated quantum chips.

Connecting multiple quantum nodes together to build a quantum internet can create more potential for quantum information processing [1, 2]. Optical quantum memories, which can hold the input optical state for on-demand reading, are able to synchronize quantum computers and implement long-distance quantum communication, making them vital for quantum networks [3]. Similar to that a quantum computer needs many qubits to demonstrate its quantum supremacy [4], network applications also impose scalability as a basic requirement for quantum memories.

Rare earth doped solids feature with long spin coherence time and large inhomogeneous linewidth [5], making them one of the best candidates for building compact quantum memories on a chip [2]. Though there have been impressive attempts to build optical memories by patterning micro/nano photonic structures on rare-earth doped crystals [6–9], combining faithful performance and easy scalability remains an unsolved problem. For example, due to the physical size of waveguide architecture, it is very difficult to achieve a high optical absorption and a high storage efficiency within μm length [8]. Increasing the density of doped ions seems a straightforward method to increase absorption efficiency, but at the cost of coherence time due to the dephasing effects caused by reduced ion-ion distance [10]. Introducing optical cavities to enhance the light-matter interaction is promising in achieving 100% storage efficiency [11, 12]. However, many quantum memory protocols such as atomic frequency comb (AFC) [13, 14], controlled reversible inhomogeneous broadening (CRIB) [15–17], and gradient echo memory (GEM) [18] relies on optical pumping and/or preparing steps. This means that in addition to requiring large optical depth for high efficiency, little dephasing for long coherence time, and large inhomogeneous linewidth for multimode capacity, these protocols ask more on the electric or magnetic properties from working ions for on-demand control. Putting so many constraints on memories ions hinders their nanophotonic implementation to take the advantage of large enhance-

ment on light-matter interaction, making on-chip quantum memories much less competitive on performance to their bulk counterparts[19, 20].

Lithium-niobate (LN) is a material that has the name of photonic silicon, famous for its large electro-, nonlinear-, and acousto-optic coefficients. Photonic devices based on thin film LN have rapidly advanced with the commercialization of lithium-niobate on insulators (LNOI). For example, the development of LN waveguides [21, 22], high-quality micro-resonators [23, 24], high-frequency modulators [25, 26], and on-chip telecom lasers [27, 28] has made thin film LN a unprecedented platform for integrated photonic circuits for both classical and quantum applications.

Instead of imposing excessive requirements to atoms that function as a memory, we propose a scheme based on $\text{Er}^{3+}:\text{LiNbO}_3$ to realize optical quantum memories by using the electro-optic effect of LN. The scheme relies a electrically tuned cavity to control the emission of photon echos, namely Cavity-Controlled Echo (CACE). The memory read-out is switchable by applying a direct-current (DC) electric field to shift the cavity frequency, giving rise to a near unit storage efficiency and low noise performance. Besides the obvious industrial advantages introduced by thin film LN and the $1.5\mu\text{m}$ telecom wavelength, this protocol not only avoids complicated preparation steps, but also can take full advantages of the long coherence time of erbium ions, the nanophotonic enhancement of light-matter interaction, and the electric tunability LN. As this scheme is favorable for on-chip electronic operation, it is easy to scale up with independent electronic control, showing potential applications in quantum photonic chips to connect multiple quantum processors.

The setup that we consider is shown diagrammatically in Fig. 1. A photonic-crystal nano-beam cavity is fabricated in a $\text{Er}^{3+}:\text{LiNbO}_3$ thin film. Through a grating coupler light is input into (and output from) the one-sided cavity. Adjacent electrodes are used to supply electric field to change the refractive index of lithium-niobate and thus the cavity resonant frequency Δ_c .

Similar to photon-echo quantum memories[29–32], our approach is modified from two-pulse echo scheme. Two-pulse echo is not suitable for optical quantum storage, be-

* stephen.chen@bit.edu.cn

† zhangxd@bit.edu.cn

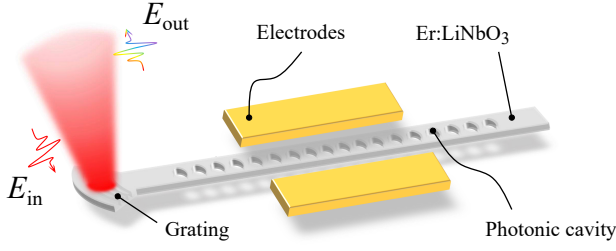


FIG. 1. Schematic of the quantum memory protocol based on cavity-controlled echo. Photonic crystal structures are fabricated on a $\text{Er}^{3+}:\text{LiNbO}_3$ thin film, which forms a nano-beam cavity. A grating coupler enables light input and output of the cavity. A pair of electrodes located on two sides of the cavity are used to shift the cavity frequency on or off resonance with stored collective atomic polarization.

cause the echo is emitted from a population-inverted medium, the gain and spontaneous emission of which ruin the echo fidelity[29, 33, 34]. Applying a second π pulse is able to bring atoms back to their ground states; therefore a secondary echo rephased by the second π pulse can be used as a readout of the stored quantum information. However the echo rephased by the first π pulse already emits a large part of the absorbed energy, leading to the efficiency reduction of the second-echo emission. To utilize the second echo as a memory readout, one needs to eliminate the emission of the first one. Some protocols take advantage of the spacial phase mismatching effect (Revival of Silenced Echo scheme, ROSE)[30], the electric Stark effect (Hybrid Photon Echo Rephasing scheme, Hyper)[31], and the light induced frequency shift effect (Light Shift Photon Echo Rephasing scheme, Lisper)[32]. In this research by applying a DC field to the LN nano-beam cavity at appropriate time, due to the electric-optic effect of LN, one can shift the resonant frequency of the cavity and thus silence the undesired echo.

The width and the thickness of the designed nano-beam cavity are $w = 900$ nm and $h = 390$ nm, respectively. Photonic bandgap around $1.5 \mu\text{m}$ is obtained by milling oval holes with $h_x = 110$ nm, $h_y = 245$ nm and a period of $p = 530$ nm, as illustrated in Fig 2(a). Cavity resonance is formed by varying the period of the five holes in the center to $p = 460$ nm. Figure 2(b) shows the simulated electric-field distribution of the cavity at the resonant wavelength of $1.5 \mu\text{m}$.

The effective refractive index of LN, for the sake of brevity, is simplified as $n_{\text{eff}} = n_0 - \frac{1}{2}n^3rE$, where $n_0 = 2.21$ [35] is the LN refractive index when no voltage is applied, $r = 30.9 \times 10^{-12} \text{m/V}$ is a constant based on the electro-optic coefficient of LN, and E is the applied DC electric field. According to our simulation, the cavity frequency Δ_c shifts linearly with the change of refractive-index $\Delta_c \propto \Delta n_{\text{eff}}$, as shown in Fig.2(c). In our calculations, applying 10 V voltage to the structure can shift the frequency approximately 60 GHz.

Since the cavity frequency can be electrically shifted, according to the Purcell effect[36], emission of atomic ensemble can either be suppressed if Δ_c is off resonant with the atomic frequency δ_a , or enhanced if Δ_c is on-resonance with δ_a . Based on this effect, we can both silence the unwanted echo

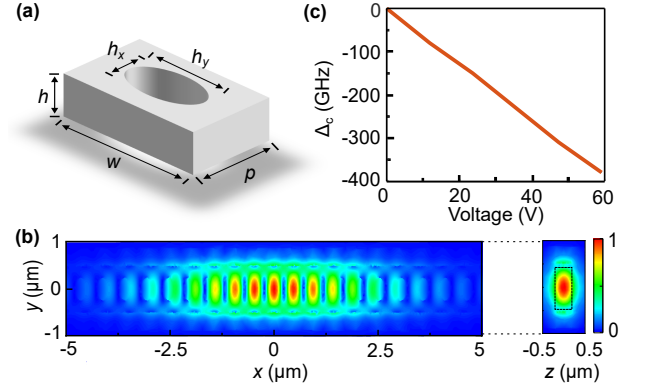


FIG. 2. Simulation of nano-beam cavity. (a)The structure of a periodic unit with dimensions as noted. (b)Simulated electric field distribution of the nano-beam cavity. Left, $x-y$ plane from top view; right, $y-z$ cross-sectional plane from side view. (c)The cavity frequency shift Δ_c as a function of applied voltage, where the space distance between two electrodes is set to be $4 \mu\text{m}$.

and enhance the secondary echo to build a high-efficiency optical quantum memory.

For a collection of N two-level erbium ions interacting with an optical cavity mode, the equation of motion for an ion is described by:

$$\begin{aligned}\dot{\rho}_{21} &= (-i\delta_a - \frac{1}{T_2})\rho_{21} + ig a(\rho_{11} - \rho_{22}), \\ \dot{\rho}_{22} &= (-\frac{1}{T_1})\rho_{22} + ig a\rho_{12} - ig a^\dagger \rho_{21}.\end{aligned}\quad (1)$$

where $\rho_{ij} = \rho_{ji}^*$ are the elements of two-level density matrix ρ , a is the cavity operator, δ_a is the atomic frequencies detuned with respect to input laser frequency ω , T_1 is the excited-state lifetime, T_2 is the optical coherence time, and g denotes the single-photon Rabi frequency. It is assumed in the above equations that the cavity and atomic operators are uncorrelated, which is a good approximation even in the single excitation regime. The detuning δ_a is inhomogeneous and subject to Gaussian distribution. We define an ensemble polarization term as

$$P = N \int_{-\infty}^{+\infty} \rho_{21}(\delta_a) G(\delta_a - \delta_0) d\delta_a, \quad (2)$$

where N is the total number of erbium ions, $G(\delta_a - \delta_0)$ is the Gaussian inhomogeneous distribution of erbium ions with δ_0 being the line center, and $\int G(\delta_a - \delta_0) d\delta_a = 1$.

For a low loss nano-beam cavity, coupling loss κ is dominant in determining the linewidth of the cavity. The equation of motion for the cavity mode is

$$\dot{a} = (-i\Delta_c - \frac{\kappa}{2})a + \sqrt{\kappa}A_{in} + igP, \quad (3)$$

where A_{in} is the input driving field (the input pulse or the control π pulse in our case). It can be seen that the polarization term P in Eq.(2) can induce both loss and dispersion to the cavity mode a . The dispersive frequency shift can be ignored

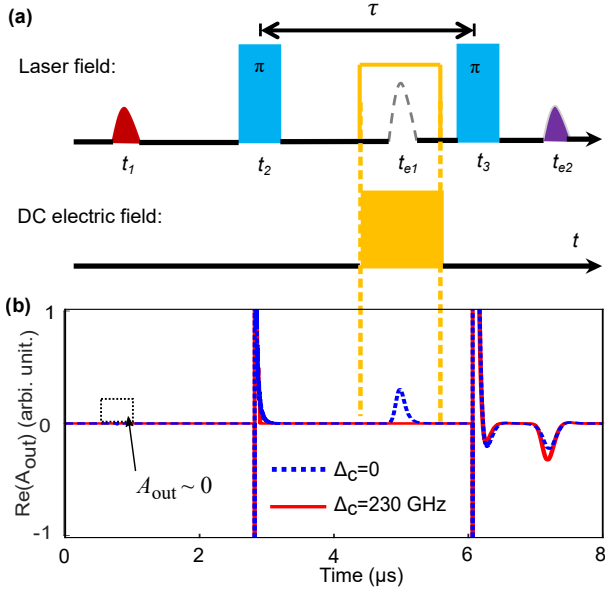


FIG. 3. Pulse sequence. (a) The pulse sequence consisting of laser field (red and blue) and external electric field (gold). The first echo between two π -pulses has been silenced by external electric field at t_{e1} . The second echo (purple) that we need is emitted at t_{e2} . Simulated electric mode in top view. (b) The output field of the pulse sequence with or without external electric field applied around the time at which the two-pulse echo is formed.

because it can easily be compensated for by changing the input laser frequency.

To get an intuitive picture of the requirements of CACE, we first consider an input laser pulse with a linewidth much narrower than κ . In such case the field inside the cavity can instantaneously follow the variation of the signal field, i.e., the adiabatic approximation $\dot{a} = 0$ applies. Further noting that the cavity input-output relation is

$$A_{\text{out}} + A_{\text{in}} = \sqrt{\kappa} a, \quad (4)$$

at the emission stage where the input A_{in} is absent, one can write the output of the cavity as

$$A_{\text{out}} = \frac{\sqrt{\kappa}}{i\Delta_c + \frac{\kappa}{2}} igP. \quad (5)$$

The polarization term P in Eq.(5) originates from the stored collective excitation of erbium ions. It is clear now if Δ_c can be detuned to a value larger than κ , the output echo can be effectively suppressed.

The CACE scheme is based on electrically tuning Δ_c . The pulse sequences of the control optical pulses and the applied voltage are illustrated in Fig. 3(a):

- I. At $t = t_0$, an optical pulse, which is the pulse needs to be stored, enters the cavity. By carefully designing a grating coupler whose coupling loss is characterized by κ and choosing a proper density of erbium ions N , impedance matching condition can be reached and the

input pulse can be perfectly absorbed.

- II. At $t = t_1$, a rephasing π -pulse is applied to the erbium ion ensemble, which reverses the phase of $\rho_{21}(\delta_a)$.
- III. At $t = t_{e1}$, where $t_{e1} - t_2 = t_2 - t_1$, the coherence ρ_{21} with respect to different δ_a restores in phase again and stimulates, if no voltage is applied, an echo emission into the LN cavity. As aforementioned this echo is noisy and not suitable for quantum memories[? ?]. To silence this echo, an external electric field is applied between t_1 and t_2 to shift the cavity frequency Δ_c out of resonance with the repahsed polarization P , whose frequency is the same as the input pulse in t_1 .
- IV. At $t = t_3$, where $t_3 - t_2 = \tau$, a second π -pulse is applied to cancel the phase differences accumulated in the period between $t_3 - t_{e2}$, and, more importantly, to bring those ions excited by the first π pulse back to their ground states.
- V. At $t = t_{e2}$, where $t_{e2} - t_3 = t_3 - t_{e1}$, a secondary echo is emitted out from the cavity in a low-noise environment.

To show that efficient storage is experimentally feasible, we calculate the output of the CACE scheme by numerically solve Eq. (1)-(4). Note that in numerical calculations aforementioned assumptions in explaining the proposal are all relaxed. A nano-beam cavity as shown in Fig. (2) is fabricated in an $\text{Er}^{3+}:\text{LiNbO}_3$ thin film, the loaded quality-factor of which is $Q = 9 \times 10^4$ (the intrinsic Q in simulations can be as high as 5×10^6), and the model volume of which is $V = 0.19 \mu\text{m}^3$. The inhomogeneous linewidth of erbium ion LN is $\Gamma_{\text{in}} \approx 180 \text{ GHz}$, the optical coherence time is $T_2 = 0.08 \text{ ms}$, and the electric dipole moment is $d_{12} = 3.5 \times 10^{-32} \text{ C} \cdot \text{m}$ [37].

The performance of the CACE scheme with (red line) and without (blue dashed line) an applied voltage is shown in Fig. 3(b). At t_0 , a light pulse with duration of $0.08 \mu\text{s}$ is input to the cavity. To obtain a high efficiency quantum storage, we need perfect absorption of the input pulse. For weak input pulse such as few photon states (where $\rho_{11} - \rho_{22} \approx 1$ applies), the polarization term $igP = -\Gamma a/2$ is a linear function of the cavity field a with Γ being a constant. As aforementioned, if the bandwidth of the input pulse is much narrower than κ , the cavity mode a can instantaneously follow the change of the input pulse. From Eq. (3) and (4) we then obtain

$$A_{\text{out}}(t) = \frac{-i\Delta_c + \frac{\kappa}{2} - \frac{\Gamma}{2}}{i\Delta_c + \frac{\kappa}{2} + \frac{\Gamma}{2}} A_{\text{in}}(t) \quad (6)$$

When $\Delta_c = 0$, there is impedance-matching $\kappa = \Gamma$ leading to ideal absorption of the input pulse. In other words, the light enters the cavity are completely absorbed and stored as a collective excitation of the erbium ions without being reflected out. That is to say, for a given κ and mode volume, we can always choose a proper erbium concentration n_{Er} to do so. In experiments this can be achieved by working at different position of the erbium inhomogeneous line. Based on the analysis above we set the concentration of erbium ion as 205 ppm and the impedance matching is confirmed in Fig. 3(b), where the output at t_0 is $A_{\text{out}}(t_0) \sim 0$.

When the applied DC field is absent, as shown in the blue dashed line in Fig. 3(b), both a primary echo and a secondary

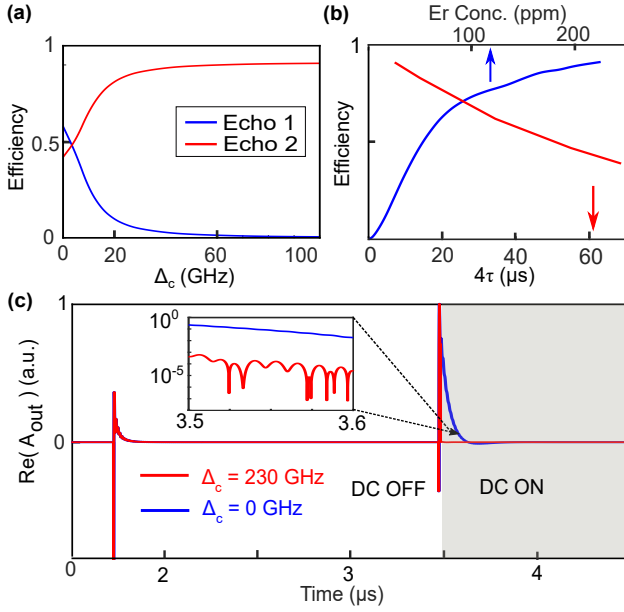


FIG. 4. Memory efficiency and noise. (a) Efficiencies of the first and second echo as a function of Δ_c . Δ_c results from the refractive index change of LN, which is introduced by the external electric field. (b) Efficiency as a function of 2τ . The maximum efficiency in the scheme is limited by the T_2 of erbium ions, which is chosen to be $80 \mu\text{s}$ in calculations. η depends on τ through an exponential function $\exp(-2\tau/T_2)$. (c) Efficiency as a function of erbium concentration. Note that in obtaining (c), together with increasing N , the duration of π pulse is adjusted accordingly. (d) Noise analysis without input field. The noise level with and without applied external electric field are shown in solid blue and solid red line. The noise caused by the FID tail of a π -pulse can be significantly reduced when switching on a large Δ_c (dashed black). The inset shows the noise ratio of two situations with $\Delta_c = 0$ and $\Delta_c = 230 \text{ GHz}$.

echo can be seen after applying π pulses to the system. However, if an electrical field is turned on to shift Δ_c 230 GHz out of resonance during the emission period of the first echo, the first echo can be silenced to a negligible level. At the same time the amplitude of the second echo, compared to its counterpart without an applied electric field, is enhanced, as shown in Fig. 3(b). Following the analysis in Eq. (3) and (5), the emission efficiency of the echo at $t = t_3$ is:

$$\eta = \left| \frac{\frac{\kappa\Gamma}{2}}{(i\Delta_c + \frac{\kappa}{2})(i\Delta_c + \frac{\kappa}{2} + \frac{\Gamma}{2})} \right|^2 \quad (7)$$

where $\eta = 1$ holds with $\Delta_c = 0$ and impedance matching $\kappa = \Gamma$.

According to Eq (5) and (6), one needs a large Δ_c to effectively cancel the first echo. In Fig. 4(a), we compare the emission efficiency of the two echos for increasing Δ_c . When there is no external DC field, the sum efficiency of the first and the second echo exceed unity because of the issue of population inversion. With increasing Δ_c , the efficiency of the second echo rises up to 92%, accompanied by the decreasing of the first one. According to Eq. (6), to obtain a high-contrast ratio between the first and the second echo, Δ_c is required to

be larger than the cavity linewidth κ (2 GHz in our case) rather than the inhomogeneous linewidth of erbium ions (180 GHz in our case). This is evident in Fig. 4(a), where for $\Delta_c \approx 60 \text{ GHz}$ the ratio between the first echo and the second echo is 1.3%.

The efficiency η of such a revival echo scheme is limited by the homogeneous linewidth of erbium ions. As shown by the red line in Fig. 4(b), if the interval 2τ between the input pulse and the revival echo is increased, the efficiency decays with respect to the decoherence time $\eta = \exp(-\frac{2\tau}{T_2})$. This is because the longer the interval 2τ is, the more ions become decoherent and cannot be rephased by π -pulses. The dependence of η on erbium concentration n_{Er} is shown by the blue line in Fig. 4(b). For a cavity with given mode volume and coupling loss, optimized η requires the impedance matching $\kappa = \Gamma$ as shown in Eq (6). This can be achieved by changing the Er^{3+} concentration, because the polarization term $P = N \int \rho_{21} G d\delta_a$ depends on n_{Er} . Note that when n_{Er} is changed, the strength or the duration of the control π pulses in calculations also need to be adjusted accordingly.

Devices for quantum applications need to be noiseless. For quantum memories based on photon echos, typical noise originates from free induction decay (FID) or spontaneous emission of π -pulses. Detuned cavity can also be used to suppress the FID noise to a negligible level. Shown in Fig. 4(c) is the output without the presence of an input signal pulse. Without an applied electric field, the FID tails of both π pulses immediately arise when the laser is switched off, as shown in the blue curve of Fig. 4(c). If an electric field is applied after the second π pulse to shift the cavity frequency 230 GHz, both the FID tail and the spontaneous emission from the π pulse (red curve) are suppressed. In our calculations, a ratio of 10^4 between the noise levels with and without an applied field can be obtained, as shown in the inset of Fig. 4(d). In a word, the noise can be switched off whenever needed.

In the CACE scheme the primary echo is silenced by the Δ_c . This is quite different with other protocols such as ROSE, CRIB and Hyper, where echo cancellation is the result of a vanishing ensemble polarization due to the destructive interference of ions with different accumulated phase (spatial or temporal). At the moment t_{e1} of CACE, all ions are already rephased, which means that an ensemble polarization is already built up and can otherwise emit photons if Δ_c is in tune. The silenced echo is based on the Purcell effect instead of the out-of-phase superposition of ions.

The control of echos and the suppressed noise are all resultant from cavity-matter interaction mediated by the LN electro-optical effect. CACE scheme assigns the requirements of quantum memories on coherence and controllability to different materials and thus brings in lots of benefits. Besides the obvious advantages such as industrial mutuality of LN fabrications and working in telecom band, easy to implement seems to be the most important one. Those protocols relying on preparation steps, such as CRIB, GEM and AFC, not only bring in technical difficulties, but more importantly, impose additional requirements on working ions. For example, in addition to the requirements on coherence properties of working ions, CRIB requires ions to have strong Stark effect to be able to introduce controllable linewidth broadening. AFC protocol

TABLE I. The results of theoretical speculation for single-atom quantum memory.

Q	V(μm^3)	Er conc.(ppm)	N_h	Efficiency(%)
2×10^5	0.28	105	3.1	91
3×10^5	0.3	70	2.2	91
4×10^5	0.28	50	1.5	91
8×10^5	0.26	26	0.7	91
7×10^6	0.23	3	0.07	91

only works for ions with long ground state lifetimes, so that a comb in absorption line can be prepared. In CACE, all these requirements are relaxed. When building a memory one can just focus on choosing those ions with great coherence times, i.e., the longest coherence time, rather than distracted by any electric or magnetic properties of the working ions.

Another benefit is that the scheme doesn't waste any absorbing ions. While most quantum memory schemes require large optical depth to get a high efficiency, those schemes relying on optical pumping, e.g., CRIB and AFC, reduce the number of absorbing ions and results in efficiency reduction. Similar as ROSE, the present process does not waste any ions initially present within the signal band-width. At the same time using a high Q cavity can further enhance the light-matter interaction and push the efficiency approaching unity.

For high Q cavities, less erbium ions are needed to achieve impedance matching condition, which, together with the small mode volume of photonic crystal cavities, enables us to exploit the possibility of the quantum memory based on single ions. We perform numerical calculated η for several combinations of Q and erbium concentrations n_{Er} , as shown in Table ???. Note that in these calculations, the mode volume V and the duration of the two π pulses are also adjusted to maintain the efficiency $\eta > 95\%$. The number of ions that can be resolved in its homogeneous linewidth is approximated by $N_h = n_{Er} * V\Gamma_h/\Gamma_{in}$, where n is the density of erbium ions, $\Gamma_h = 1/(\pi T_2) = 1$ MHz is the homogeneous linewidth [37], and Γ_{in} is the inhomogeneous linewidth. For $Q \approx 10^5$, the number of interacting erbium ion can easily be reduced to single digit. For erbium samples with a Gaussian broadening,

working on the edge of the inhomogeneous line can further reduced N_h and facilitate single ion detection. Quantum memories using single ions system has several advantages, e.g., the addressable property of a single ion can be used to predict whether the information has been successfully stored [38, 39], and deterministic entanglement can be established [40, 41]. With decreasing erbium concentration, CACE shows the potential of realizing solid-state single-ion quantum memories.

In this paper, we propose a on-chip quantum memory scheme named cavity-controlled echo by utilizing the electric-optic effect of lithium niobate. The numerical results show that the echo readout efficiency approaches unity by applying a voltage to control the frequency of a photonic crystal cavity on a LiNbO₃ thin film. Nanophotonic cavities feature with large Purcell effect, and thus can be used to enhance the efficiency of memories. The scheme offers new degrees of freedom in exploiting quantum memories, such as noise suppression by applied DC field and single-ion quantum memories.

Compared with the difficulty of tailoring the inhomogeneous absorption linewidth that is needed for CRIB, GEM and AFC, the tunability by electric field in lithium niobate is industrially mutual. Its experimental realization, especially on a chip, is much easier. For example, the LN waveguide loss can be as low as 0.01 dB/cm; and the Q factor of the LN cavity approaches 10^8 [42]. Patterning waveguides, cavities, and routers on Er³⁺:LiNbO₃ is much the same. We thus expect that this memory scheme is as scalable as other LN devices, enabling more and more quantum memories to be loaded to a network. Erbium ions in LN shows a coherence time on the order of 100 μs [37], and by using of the ground state spin levels the coherence time can be further extended to the order of seconds [43–45]. We therefore expect it is experimentally feasible in building an integrated quantum memory with high efficiency and long coherence time on Er³⁺:LiNbO₃ thin film.

The authors wish to acknowledge financial support from the Start-up Fund of Beijing Institute of Technology, the Science and Technology Innovation Project of Beijing Institute of Technology, and National Natural Science Foundation of China (No. 62105033 and No. 12174026).

[1] C. Simon, "Towards a global quantum network," *Nature Photonics*, vol. 11, no. 11, pp. 678–680, 2017.
[2] T. Zhong and P. Goldner, "Emerging rare-earth doped material platforms for quantum nanophotonics," *Nanophotonics*, vol. 8, pp. 2003–2015, sep 2019.
[3] A. I. Lvovsky, B. C. Sanders, and W. Tittel, "Optical quantum memory," *Nature Photonics*, vol. 3, no. 12, pp. 706–714, 2009.
[4] F. Arute, K. Arya, R. Babbush, D. Bacon, J. C. Bardin, R. Barends, R. Biswas, S. Boixo, F. G. S. L. Brandao, D. A. Buell, B. Burkett, Y. Chen, Z. Chen, B. Chiaro, R. Collins, W. Courtney, A. Dunsworth, E. Farhi, B. Foxen, A. Fowler, C. Gidney, M. Giustina, R. Graff, K. Guerin, S. Habegger, M. P. Harrigan, M. J. Hartmann, A. Ho, M. Hoffmann, T. Huang,

T. S. Humble, S. V. Isakov, E. Jeffrey, Z. Jiang, D. Kafri, K. Kechedzhi, J. Kelly, P. V. Klimov, S. Knysh, A. Korotkov, F. Kostritsa, D. Landhuis, M. Lindmark, E. Lucero, D. Lyakh, S. Mandrà, J. R. McClean, M. McEwen, A. Megrant, X. Mi, K. Michielsen, M. Mohseni, J. Mutus, O. Naaman, M. Neeley, C. Neill, M. Y. Niu, E. Ostby, A. Petukhov, J. C. Platt, C. Quintana, E. G. Rieffel, P. Roushan, N. C. Rubin, D. Sank, K. J. Satzinger, V. Smelyanskiy, K. J. Sung, M. D. Trevithick, A. Vainsencher, B. Villalonga, T. White, Z. J. Yao, P. Yeh, A. Zalcman, H. Neven, and J. M. Martinis, "Quantum supremacy using a programmable superconducting processor," *Nature*, vol. 574, pp. 505–510, oct 2019.
[5] C. Thiel, T. Böttger, and R. Cone, "Rare-earth-doped materials

- for applications in quantum information storage and signal processing,” *Journal of Luminescence*, vol. 131, pp. 353–361, mar 2011.
- [6] T. Zhong, J. M. Kindem, J. G. Bartholomew, J. Rochman, I. Craiciu, E. Miyazono, M. Bettinelli, E. Cavalli, V. Verma, S. W. Nam, F. Marsili, M. D. Shaw, A. D. Beyer, and A. Faraon, “Nanophotonic rare-earth quantum memory with optically controlled retrieval,” *Science*, vol. 1395, no. September, pp. 1392–1395, 2017.
 - [7] T. Zhong, J. M. Kindem, E. Miyazono, and A. Faraon, “Nanophotonic coherent light–matter interfaces based on rare-earth-doped crystals,” *Nat. Commun.*, vol. 6, no. 8206, 2015.
 - [8] C. Liu, Z. Q. Zhou, T. X. Zhu, L. Zheng, M. Jin, X. Liu, P. Y. Li, J. Y. Huang, Y. Ma, T. Tu, T. S. Yang, C. F. Li, and G. C. Guo, “Reliable coherent optical memory based on a laser-written waveguide,” *Optica*, vol. 7, no. 2, pp. 192–197, 2020.
 - [9] E. Saglamyurek, N. Sinclair, J. Jin, J. A. Slater, D. Oblak, W. Tittel, F. Bussières, M. George, R. Ricken, and W. Sohler, “Broadband waveguide quantum memory for entangled photons,” *Nature*, vol. 469, pp. 512–515, 2010.
 - [10] Y.-H. Chen, S. P. Horvath, J. J. Longdell, and X. Zhang, “Optically Unstable Phase from Ion-Ion Interactions in an Erbium-Doped Crystal,” *Physical Review Letters*, vol. 126, p. 110601, mar 2021.
 - [11] S. A. Moiseev, S. N. Andrianov, and F. F. Gubaidullin, “Efficient multimode quantum memory based on photon echo in an optimal QED cavity,” *Physical Review A*, vol. 82, p. 022311, aug 2010.
 - [12] M. Afzelius and C. Simon, “Impedance-matched cavity quantum memory,” *Physical Review A - Atomic, Molecular, and Optical Physics*, vol. 82, no. 2, pp. 1–4, 2010.
 - [13] C. Liu, T. X. Zhu, M. X. Su, Y. Z. Ma, Z. Q. Zhou, C. F. Li, and G. C. Guo, “On-demand quantum storage of photonic qubits in an on-chip waveguide,” *Phys. Rev. Lett.*, vol. 125, p. 260504, 2020.
 - [14] I. Craiciu, M. Lei, J. Rochman, J. M. Kindem, J. G. Bartholomew, E. Miyazono, T. Zhong, N. Sinclair, and A. Faraon, “Nanophotonic quantum storage at telecommunication wavelength,” *Phys. Rev. Applied*, vol. 12, p. 024062, 2019.
 - [15] B. Kraus, W. Tittel, N. Gisin, M. Nilsson, and J. I. Cirac, “Quantum memory for nonstationary light fields based on controlled reversible inhomogeneous broadening,” *Phys. Rev. A*, vol. 73, no. 2, pp. 164–164, 2005.
 - [16] B. Lauritzen, J. Minář, H. De Riedmatten, M. Afzelius, N. Sangouard, C. Simon, and N. Gisin, “Telecommunication-wavelength solid-state memory at the single photon level,” *Phys. Rev. Lett.*, vol. 104, p. 080502, 2010.
 - [17] J. J. Longdell and M. J. Sellars, “Analytic treatment of controlled reversible inhomogeneous broadening quantum memories for light using two-level atoms,” *Phys. Rev. A*, vol. 78, no. 3, 2008.
 - [18] D. B. Higginbottom, B. M. Sparkes, M. Rancic, O. Pinel, M. Hosseini, P. K. Lam, and B. C. Buchler, “Spatial mode storage in a gradient echo memory,” *Phys. Rev. A*, vol. 86, no. 2, pp. 1955–1963, 2012.
 - [19] Y. C. Ho, G. T. C. Ampbell, J. L. E. Verett, J. B. Ernu, D. B. H. Iggibottom, M. T. C. Ao, J. G. Eng, N. P. R. Obins, P. K. L. Am, and B. C. B. Uchler, “Highly efficient optical quantum memory with long coherence time in cold atoms,” vol. 3, no. 1, 2016.
 - [20] J. Dajczgewand, J. L. Le Gouët, A. Louchet-Chauvet, and T. Chanelière, “Large efficiency at telecom wavelength for optical quantum memories,” *Opt. Lett.*, vol. 39, no. 9, pp. 2711–2714, 2014.
 - [21] S. Wang, L. Yang, R. Cheng, Y. Xu, and H. X. Tang, “Incorporation of erbium ions into thin-film lithium niobate integrated photonics,” *Appl. Phys. Lett.*, vol. 116, no. 15, p. 151103, 2020.
 - [22] V. Y. Shur, A. R. Akhmatkhanov, and I. S. Baturin, “Micro- and nano-domain engineering in lithium niobate,” *Appl. Phys. Rev.*, vol. 2, no. 4, p. 040604, 2015.
 - [23] J. Wang, F. Bo, S. Wan, W. Li, F. Gao, J. Li, G. Zhang, and J. Xu, “High-q lithium niobate microdisk resonators on a chip for efficient electro-optic modulation,” *Opt. Express*, vol. 23, no. 18, p. 23072, 2015.
 - [24] M. Wang, Y. Xu, Z. Fang, Y. Liao, P. Wang, W. Chu, L. Qiao, J. Lin, W. Fang, and Y. Cheng, “On-chip electro-optic tuning of a lithium niobate microresonator with integrated in-plane microelectrodes,” *Opt. Express*, vol. 25, no. 18, pp. 124–129, 2017.
 - [25] M. Li, J. Ling, Y. He, U. A. Javid, and Q. Lin, “Lithium niobate photonic-crystal electro-optic modulator,” *Nat. Commun.*, vol. 11, no. 1, 2020.
 - [26] W. Cheng, M. Zhang, B. Stern, M. Lipson, and M. Loncar, “Nanophotonic lithium niobate electro-optic modulators,” *Opt. Express*, vol. 26, pp. 1547–1555, 2018.
 - [27] Z. Wang, Z. W. Fang, Z. X. Liu, W. Chu, Y. Zhou, J. H. Zhang, R. B. Wu, M. Wang, T. Lu, and Y. Cheng, “On-chip tunable microdisk laser fabricated on Er^{3+} -doped lithium niobate on insulator,” *Opt. Lett.*, vol. 46, no. 2, pp. 380–383, 2021.
 - [28] Q. Luo, C. Yang, R. Zhang, Z. Z. Hao, D. H. Zheng, H. D. Liu, X. Y. Yu, F. Gao, F. Bo, Y. Kong, G. Q. Zhang, and J. Xu, “On-chip erbium-doped lithium niobate microring lasers,” *Opt. Lett.*, vol. 46 13, pp. 3275–3278, 2021.
 - [29] S. A. Moiseev and B. S. Ham, “Photon-echo quantum memory with efficient multipulse readings,” *Physical Review A*, vol. 70, p. 063809, dec 2004.
 - [30] V. Dameron, M. Bonarota, A. Louchet-Chauvet, T. Chanelière, and J. Gouët, “Revival of silenced echo and quantum memory for light,” *New J. Phys.*, vol. 13, no. 9, p. 093031, 2011.
 - [31] D. L. Mcauslan, P. M. Ledingham, W. R. Naylor, S. E. Beavan, and J. J. Longdell, “Photon-echo quantum memories in inhomogeneously broadened two-level atoms,” *Phys. Rev. A*, vol. 84, no. 2, pp. 8767–8777, 2011.
 - [32] H. C. McDonald, “Controlling photon echoes with the light shift,” *Master’s thesis*, 2016.
 - [33] J. Ruggiero, J. Gouët, C. Simon, and T. Chanelière, “Why the two-pulse photon echo is not a good quantum memory protocol,” *Phys. Rev. A*, vol. 79, no. 5, pp. 1744–1747, 2008.
 - [34] P. M. Ledingham, W. R. Naylor, and J. J. Longdell, “Nonclassical photon streams using rephased amplified spontaneous emission,” *Phys. Rev. A*, vol. 81, no. 1, pp. 116–116, 2010.
 - [35] A. Pan, C. R. Hu, C. Zeng, and J. S. Xia, “Fundamental mode hybridization in a thin film lithium niobate ridge waveguide,” *Opt. Express*, vol. 27, no. 24, pp. 35659–35669, 2019.
 - [36] E. M. Purcell, “Spontaneous emission probabilities at radio frequencies,” 1946.
 - [37] C. W. Thiel, R. M. Macfarlane, T. Böttger, Y. Sun, R. L. Cone, and W. R. Babbitt, “Optical decoherence and persistent spectral hole burning in $\text{Er}^{3+}:\text{LiNbO}_3$ - sciencedirect,” *J. Lumin.*, vol. 130, no. 9, pp. 1603–1609, 2010.
 - [38] N. Piro, F. Rohde, C. Schuck, M. Almendros, J. Huwer, J. Ghosh, A. Haase, M. Hennrich, F. Dubin, and J. Eschner, “Heralded single-photon absorption by a single atom,” *Nat. Physics*, vol. 7, no. 1, pp. 17–20, 2011.
 - [39] H. P. Specht, C. N?lleke, A. Reiserer, M. Uphoff, E. Figueroa, S. Ritter, and G. Rempe, “A single-atom quantum memory,” *Nature*, vol. 473, no. 7346, p. 190, 2011.
 - [40] J. I. Cirac, P. Zoller, H. J. Kimble, and H. Mabuchi, “Quan-

- tum state transfer and entanglement distribution among distant nodes in a quantum network,” *Phys. Rev. Lett.*, vol. 78, no. 16, pp. 3221–3224, 1996.
- [41] W. Tatjana, S. C. Webster, A. Kuhn, and G. Rempe, “Single-atom single-photon quantum interface,” *Science*, vol. 317, no. 16, pp. 488–490, 2007.
- [42] T. J. Wang, G. L. Peng, M. Chan, and C. H. Chen, “On-chip optical microresonators with high electro-optic tuning efficiency,” *J. Lightwave Technol.*, vol. 38, no. 7, pp. 1851–1857, 2020.
- [43] M. Rančić, M. P. Hedges, R. L. Ahlefeldt, and M. J. Sellars, “Coherence time of over a second in a telecom-compatible quantum memory storage material,” *arXiv*, 2016.
- [44] Y.-H. Chen, X. Fernandez-Gonzalvo, and J. J. Longdell, “Coupling erbium spins to a three-dimensional superconducting cavity at zero magnetic field,” *Physical Review B*, vol. 94, p. 075117, aug 2016.
- [45] J. V. Rakonjac, Y. H. Chen, S. P. Horvath, and J. J. Longdell, “Long spin coherence times in the ground state and in an optically excited state of Er^{3+} 167: Y_2SiO_5 at zero magnetic field,” *Physical Review B*, vol. 101, no. 18, p. 184430, 2020.
- [46] K. Heshami, D. G. England, P. C. Humphreys, P. J. Bustard, V. M. Acosta, J. Nunn, and B. J. Sussman, “Quantum memories: emerging applications and recent advances,” *Phys. Rev. A*, vol. 63, no. 20, pp. 2005–2028, 2015.
- [47] E. Miyazono, T. Zhong, I. Craiciu, J. M. Kindem, and A. Faraon, “Coupling of erbium dopants to yttrium orthosilicate photonic crystal cavities for on-chip optical quantum memories,” *Appl. Phys. Lett.*, vol. 108, no. 1, p. 011111, 2016.
- [48] Y. H. Chen, G. F. Xavier, and J. J. Longdell, “Coupling erbium spins to a three-dimensional superconducting cavity at zero magnetic field,” *Phys. Rev. B*, vol. 94, p. 075117, 2016.
- [49] Y. Fu, M. F. Wang, and Y. Z. Zheng, “Cavity-assisted revival of silenced echo quantum memory,” *Opt. Commun.*, vol. 321, pp. 162–166, 2014.
- [50] M. M. Minnegaliev, K. I. Gerasimov, R. V. Urmancheev, and S. A. Moiseev, “Quantum memory in the revival of silenced echo scheme in an optical resonator,” *Quantum Electron.*, vol. 48, no. 10, pp. 894–897, 2018.